RSC Advances

PAPER

View Article Online
View Journal | View Issue

Cite this: *RSC Adv.*, 2019, **9**, 25667

Antibacterial performance of polymer quaternary ammonium salt–capped silver nanoparticles on *Bacillus subtilis* in water†

Jingyu Wang,[a] Minghao Sui,*[b] Zhanfang Ma,[c] Hongwei Li[d] and Bojie Yuan[e]

Received 31st July 2019
Accepted 8th August 2019

DOI: 10.1039/c9ra05944j

rsc.li/rsc-advances

In this study, we prepared polymer quaternary ammonium salt–capped silver nanoparticles (PQAS–AgNPs) and investigated their antimicrobial activities. The antimicrobial effectiveness of PQAS–AgNPs on *Bacillus subtilis* (*B. subtilis*), and the effect of dose, pH, chloride ion and humic acid (HA) were studied. It was found that PQAS–AgNPs revealed excellent antimicrobial activity to *B. subtilis*, compared with polyvinylpyrrolidone-capped silver nanoparticles (PVP-AgNPs), which was the reference antimicrobial material. The positive surface, the antimicrobial activity of PQAS, and the synergistic antibacterial effect between PQAS and AgNPs contributed to the significant antibacterial superiority of PQAS–AgNPs. This study demonstrated that the impact of the dose of the material was positive and the microbiocidal efficacy of PQAS–AgNPs was stronger at lower pH. In addition, the antibacterial performance of PQAS–AgNPs decreased in the presence of Cl^- and HA. Finally, in combination with the results of FCM and adenosine triphosphate (ATP) content, it was found that PQAS–AgNPs destroyed the respiratory chain of bacterial cells, reduced the synthesis of ATP, and destroyed the cell wall and cell membrane function.

1 Introduction

Disinfection is an obligatory process to guarantee the safety of drinking water. Traditional disinfection technology with disinfectants (*e.g.* chlorine, chloramines, ozone, and chlorine dioxide) can inactivate bacteria efficiently, but the formation of disinfection by-products (DBPs) remains a serious problem.[1] Potential health risks of DBPs from drinking water include carcinogenic, teratogenetic and mutagenic effects.[2–4] An epidemiological study has shown that 9.0% of all cases of prostate cancers and 15.0% of anal cancers are attributed to chlorinated drinking-water by-products.[5] The development of novel disinfection methods without DBPs risks has been paid more and more attention by researchers in the last two decades.[6,7]

Nanomaterials have attracted great attention for their potential use in water disinfection field, exhibiting highly antimicrobial activity and reducing the possibility of the formation of harmful DBPs.[8] Among nanomaterials, silver nanoparticles (AgNPs) are the most promising antibacterial agent. Gong *et al.* proved that AgNPs have broad inhibitory biocidal spectra for microbes including bacteria, viruses and other eukaryotic micro-organisms.[9] Dankovich *et al.* reported that AgNPs could inactivate *Escherichia coli* (*E. coli*) and *Enterococcus faecalis* (*E. faecalis*) effectively.[10] Guzman *et al.* found that AgNPs inhibited the growth and multiplication of highly multidrug-resistant bacteria such as methicillin resistant *Staphylococcus aureus* (*S. aureus*), *E. coli*, and *Pseudomonas aeruginosa* (*P. aeruginosa*).[11]

The dissolution of metallic ions and their attack on microorganisms in aqueous solution were generally proposed to be the main antimicrobial pathways for metal-type of antimicrobial nanomaterials, however, some researchers considered that the contact of bacteria with nanomaterials had a crucial influence on the inactivating efficiency. Huang *et al.* reported that the efficient inactivation capacity of nano copper loaded multiwalled carbon nanotubes (nCu-MWCNTs) on *E. coli* was mainly because MWCNTs strengthened the contact of bacteria with nCu.[12] Ma *et al.* found that in comparison with graphene oxide (GO), a significant decrease in the negative charge of Ag–GO composite which facilitated the contact between *E. coli* and Ag–GO was one of the important reasons for the improvement of the antibacterial activity of GO.[13] The surface of the bacteria in natural water is generally negatively charged. So antimicrobial

[a]*School of Environmental Science and Engineering, Tongji University, 1239 Siping Road, Shanghai 200092, People's Republic of China*

[b]*State Key Laboratory of Pollution Control and Resource Reuse, Shanghai Institute of Pollution Control and Ecological Security, School of Environmental Science and Engineering, Tongji University, 1239 Siping Road, Shanghai 200092, People's Republic of China. E-mail: minghaosui@tongji.edu.cn; Fax: +86-21-65986313; Tel: +86-21-65982691*

[c]*School of Environmental Science and Engineering, Tongji University, 1239 Siping Road, Shanghai 200092, People's Republic of China*

[d]*College of Surveying and Geo-Informatics, Tongji University, 1239 Siping Road, Shanghai 200092, People's Republic of China*

[e]*School of Environmental Science and Engineering, Tongji University, 1239 Siping Road, Shanghai 200092, People's Republic of China*

† Electronic supplementary information (ESI) available. See DOI: 10.1039/c9ra05944j

materials with positive surface which are prone to contacting with bacteria through electrostatic interaction should have better bactericidal capacity than those with negative or neutral charge. The existing studies on synthesis and antimicrobial properties of positively charged AgNPs have rarely been reported.

Quaternary ammonium salt (QAS), a positive charged antibacterial agent, is widely used as antiseptics, disinfectants, biocides, detergents, and so on.[14,15] However, these small molecules are highly toxic to the environment and their protection is short-lived.[16] During the last two decades, polymer quaternary ammonium salts (PQAS) have become a research hotspot, because it is believed that they are nonvolatile, chemically stable, and do not permeate through the skin.[17,18] Dizman *et al.* synthesized a methacrylate monomer containing pendant QAS based on 1,4-di-azabicyclo-[2.2.2]-octane (DABCO), which contained either a butyl or a hexyl group and investigated the antimicrobial activities of the corresponding small molecules (bis-quaternary ammonium monocarboxylates) and polymers. Although the small molecules did not show any antimicrobial activity, the polymers were effectively bactericidal against *S. aureus* and *E. coli* in water.[17,19]

In this work, the polymer quaternary ammonium salt–capped silver nanoparticles (PQAS–AgNPs) was prepared aiming at obtaining a kind of antibacterial nanomaterial carrying positive-charge and possessing highly antibacterial capacity by combining the inactivating capacity of PQAS and AgNPs. *Bacillus subtilis* (*B. subtilis*) was chosen as the representative bacterium in water. To the best of the authors' knowledge, there is scarcely any publications on the deactivation of *B. subtilis* under PQAS–AgNPs. *B. subtilis* is the typical bacterium used in water or wastewater disinfection experiments. *B. subtilis*, the Gram-positive bacterium, has thicker peptidoglycans layer than Gram-negative bacteria which acts as an additional barrier for the entry of disinfectors inside the cells and is more difficult to be deactivated.[20] And some water plants used *B. subtilis* as a microbial indicator for disinfection efficiency.[21] Further, *B. subtilis* has similar biological characteristics to *Cryptosporidium* or *Giardia*.[22–24] Therefore, *B. subtilis* was often used as a substitute for *Cryptosporidium* or *Giardia* to study the inactivation of the microorganisms. The results of the deactivation of AgNPs on *B. subtilis* might also provide some information on the deactivation effectiveness of nano-particles towards *Cryptosporidium* or *Giardia*, which can't be deactivated in chlorination. Besides, *B. subtilis* is not pathogenic, and colonies are easy to count. Special emphasis was placed on (1) investigating the antimicrobial efficiency of PQAS–AgNPs to *B. subtilis*; (2) examining the influencing factors, such as dose, pH, chloride ion and humic acid; and (3) exploring the damage to the *B. subtilis* cells, such as cell membrane and ATP changes.

2 Materials and methods

2.1 Materials

Silver nitrate ($AgNO_3$) were purchased from Sigma-Aldrich. Glucose, sodium borohydride ($NaBH_4$), ammonia water and anhydrous ethanol were purchased from Sinopharm (China). QAS can't combine with AgNPs *via* coordination bond, and chitosan was used as the chelator. Quaternized chitosan (QCS) (LOT: 104090, degree of substitution > 98%) was purchased from Cool Chemistry. The electrically neutral polyvinyl pyrrolidone-capped AgNPs (PVP-AgNPs) was used as the reference antibacterial material and purchased from Sigma-Aldrich (the size: 40 nm). Freeze-dried *B. subtilis* (ATCC 6633) was obtained from ATCC (USA). It was cultivated in nutrient broth (BD, USA) overnight at 37 °C in an aerobic shaker incubator with a constant agitation rate of 130 rpm. The labware and glassware used in the experiments were washed with 10% HNO_3, rinsed thoroughly with pure water and oven-dried under dust-free conditions.

2.2 Preparation of PQAS–AgNPs

PQAS–AgNPs were prepared following chemical reduction method. That was to say, in the liquid phase condition, silver ions were reduced to silver nanoparticles under the action of reductant. In order to prepare silver nanoparticles with uniform and controllable size, the crystal seed method was used. The total preparation process could be divided into four stages: solution preparation, crystal nucleus formation, crystal nucleus growth, purification and separation. Firstly, a certain concentration of solution was prepared, in which the concentration of $AgNO_3$ solution was 25.0 mmol L^{-1}, that of $NaBH_4$ was 6.25 mmol L^{-1}, that of QCS solution was 10.0 mg mL^{-1}, and that of glucose solution was 1.0 mol L^{-1}. Secondly, $AgNO_3$ solution and QCS solution were mixed in volume ratio of 1 : 5 and stirred for 5 min to obtain a white turbid solution, in which silver chloride precipitation formed. The silver ammonia solution was obtained by adding ammonia water dropwise to the turbid solution until the precipitation just disappeared. Sodium borohydride was slowly added to the silver ammonia solution in volume ratio of 6 : 1 ($AgNO_3$: $NaBH_4$). Then, the solution was transferred to three-necked flask at 95 °C and heated for one hour. Crystal seeds of PQAS–AgNPs were synthesized with the size of 4–5 nm. Thirdly, $AgNO_3$ and glucose mixed solution with volume ratio of 1 : 1 were added to the obtained crystal seeds solution and reacted at 80 °C for 30 min. When the added $AgNO_3$ volume attained a quarter of the volume of $AgNO_3$ added in prior step, the size of PQAS–AgNPs reached 40 nm approximately. Finally, the PQAS–AgNPs solution was centrifuged and separated at a high speed of 10 000 rpm for 40 min. After the supernatant was removed, the centrifuged PQAS–AgNPs were washed three times with pure water and anhydrous ethanol. Therefore, a purified polymer quaternary ammonium salt–capped silver nanoparticles composite (PQAS–AgNPs) was obtained.

2.3 Characterization of PQAS–AgNPs

UV-visible absorption spectroscopy (JiHong, China) with quartz cuvettes (1 cm optical path) as the containers was used to record the UV-visible absorption spectra. The morphology and the size of PQAS–AgNPs were determined by transmission electron microscopy (TEM, JEM-2011, Jeol, Japan), which was coupled with an energy dispersive spectrometer (EDS). X-ray

photoelectron spectroscopy (XPS) (PHI 5600, PerkinElmer Inc.) was used to determine the valence state of the produced AgNPs. The surface charge of the AgNPs was evaluated by zeta (ζ) potential, using a Zetasizer Nano instrument (Zetasizer Nano ZS 90, Malvern, UK) at 25 °C. The concentration of synthesized composite material was calculated by silver. The silver concentration was measured by an inductively coupled plasma mass spectrometry (ICP-MS7700, Agilent, USA) after being digested with concentrated HNO_3 for 2 h.

2.4 Antibacterial experiments

All antibacterial assays were performed in Class II microbiological safety cabinet (AC2-4S1, ESCO). The traditional heterotrophic plate counting (HPC) method was used to determine the viable cell numbers.[25] Briefly, 100 μL bacteria suspension with initial cell concentration of about 10^7 CFU mL^{-1} was added to 900 μL of 2 mM $NaHCO_3$ solution containing antimicrobial material. The number of viable cell was determined by spreading 30 μL of the above mixed suspension onto the nutrient agar plate for aerobic incubation at 37 °C. After 18–24 h incubation, bacterial colonies on each plate were counted. In control test, the bacteria suspension was added into 2 mM $NaHCO_3$ solution in the absence of antimicrobial material. All experiments were conducted three times. The viable cell number was calculated as colony forming units per milliliter (CFU mL^{-1}). The antibacterial rate was calculated as the equation below:

The survival rate ($\lg N_0/N$) = lg(viable cell number in control(sample without addition of antibacterial material)/viable cell number in sample(sample with addition of antibacterial material))

Zeta potential of bacterial suspension was conducted with a Zetasizer Nano instrument (Zetasizer Nano ZS 90, Malvern, UK). In order to quantify the ionic release of dissolved silver, samples were centrifuged and filtered by centrifugal ultrafilters (Amicon Ultra-15 3 K, Millipore, Billerica, MA) for 30 min at 15 000 rpm. Nominal pore size of the porous cellulose membranes was 1–2 nm, which were small enough to separate silver ion from nanoparticles. The total organic carbon (TOC) of the composite material was measured by a TOC analyzer (TOC-LCPH, Shimadzu, JP).

2.5 The analysis on the damage of *B. subtilis*

2.5.1 Flow cytometry (FCM) assay. For assessment of integrity and permeabilisation of *B. subtilis* cells, two fluorescent dyes specific for the staining of cellular nucleic acids were used: SYBR Green I (λ_{ex} = 495 nm, λ_{em} = 525 nm; provided by Solarbio, China) and propidium iodide (λ_{ex} = 536 nm, λ_{em} = 617 nm; provided by Solarbio, China), hereafter referred to as SG-I and PI respectively. SG-I could easily penetrate the membrane of the living cells and mark them green, and PI was a DNA binding dye which could only stain the dead cells with red apparent appearance.[26] FCM analysis was performed using a BD FACSVerse flow cytometer (Becton, Dickinson and Company). The stained samples were incubated for 15 min in the dark at 37 °C. All cytograms of fluorescence emissions were recorded on an exponential scale and drawn with the FlowJo software (https://www.flowjo.com/). Bacterial cells were separated from instrument noise or sample background by electronic gates, which were constructed manually using the software.

2.5.2 Determination the adenosine triphosphate (ATP) changes of cells. Total ATP concentration was measured using BacTiter-Glo reagent (G8230, Promega, America) and a luminometer (Synergy™ 4, BioTek, USA). Extracellular ATP was quantified after the filtration of the sample with 0.1 μm filter using a sterile 2 mL syringe. Intracellular ATP was calculated by subtracting extracellular ATP from total ATP.[27] One hundred microliters samples were added to 100 μL reagent, and mixed evenly. The luminescence intensity of the samples was measured after mixing for 20 s. All the measurements were done in triplicate and the standard deviation of the measurement was below 5%.

3 Results and discussion

3.1 Characterization of PQAS–AgNPs

The optical property of synthesized PQAS–AgNPs was displayed in Fig. 1(a). A single absorption peak at 418 nm was observed, which revealed the typical AgNPs optical absorbance feature.[28] The steep absorption peak reflected the good dispersion of the nanoparticles, which indicated that AgNPs had been successfully synthesized. The morphology of PQAS–AgNPs was shown

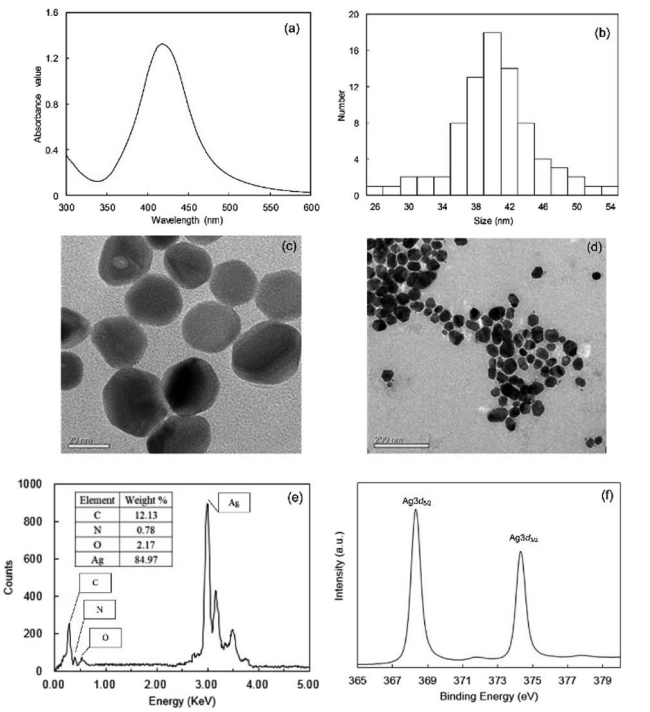

Fig. 1 Characterization of PQAS–AgNPs (a) UV-visible spectrum; (b) the size distribution; (c and d) TEM images; (e) corresponding EDS spectrum and (f) XPS spectrum.

in Fig. 1(c and d). The PQAS–AgNPs were approximately spherical in shape, well dispersed and uniform in size. A bright film could be seen on the surface of AgNPs, which indicated that PQAS had been successfully coated on the surface of nanoparticles. The EDS and XPS results further confirmed the generation of AgNPs (Fig. 1(e and f)). A distinct signal and high atomic percent values for silver were obtained from the EDS profile. The strong silver signal along with a weak carbon, oxygen and nitrogen peak might originate from PQAS that were bound to the surface of AgNPs. XPS spectrum showed that the doublet $Ag3d_{5/2}$ and $Ag3d_{3/2}$ peaks were at 368.3 eV and 374.3 eV, respectively, demonstrating that Ag mainly stayed at zero valence.[29,30] Wang reported that the surface modifier of AgNPs mainly depended on the ligand bond between lone pair electrons such as N or O in the materials and silver.[31] In PQAS, there were a large number of amino and hydroxyl groups, so PQAS could bond with AgNPs. Nanomeasure was used to determine the particle size distribution, and the results were shown in Fig. 1(b). The particle sizes were mainly distributed between 26 to 54 nm and the average value was 40 nm. The PQAS–AgNPs possessed a positive surface, and the ζ potential of PQAS–AgNPs was monitored to be +30.8 mV. The physicochemical properties of PVP-AgNPs were also studied (Fig. S1†). The size was 40 nm and the ζ potential was −9.3 mV.

3.2 Antibacterial capacity of PQAS–AgNPs

Taking PVP-AgNPs as reference, we evaluated the antibacterial capacity of PQAS–AgNPs towards *B. subtilis*. As shown in Fig. 2, PQAS–AgNPs showed a significant antibacterial superiority to PVP-AgNPs. After 5 minutes of contact with PQAS–AgNPs and PVP-AgNPs, the inactivation rates of *B. subtilis* were 1.21 log and 0.42 log, respectively. Longer contact time was beneficial to the inactivation of PVP-AgNPs and PQAS–AgNPs to *B. subtilis*, while PQAS–AgNPs still showed better antibacterial capacity than PVP-AgNPs. At 30 min, the antibacterial rate of PQAS–AgNPs was 1.26 times higher than that of PVP-AgNPs. After 60 min, the antibacterial efficiency of PVP-AgNPs increased to 2.09 log, and the inactivation rate of PQAS–AgNPs to *B. subtilis* reached 3.55 log.

The positive charge and the antimicrobial activity of PQAS should be the reason why PQAS–AgNPs possessed better antimicrobial capacity than PVP-AgNPs. The isoelectric points of bacteria were commonly between 2–5,[32] and the surface potential of bacteria in natural water was negative. Antimicrobial materials with positive charge surface should have antibacterial advantage over that with negative charge surface because of the electrostatic attraction between bacteria and the antibacterial materials. El Badawy *et al.* have studied the antimicrobial activity of several AgNPs with different surface modifiers, including uncoated H_2-AgNPs, PVP-AgNPs, citrate-AgNPs and BPEI-AgNPs (branched polyethyleneimine-coated silver nanoparticles).[33] The results showed that BPEI-AgNPs with the positive surface had the strongest bactericidal effect than the other three antibacterial materials carrying negative charge. In our experiment, the ζ potential of *B. subtilis* at pH 7.1 was measured to be −40.5 mV, and the surface potential of PQAS–AgNPs was positive with ζ potential of +30.8 mV. Compared with PVP-AgNPs with negative surface potential (ζ potential: −9.3 mV), *B. subtilis* was obviously more easily accessible to the surface of PQAS–AgNPs, which then facilitated the deactivation of *B. subtilis*.

Different from PVP, PQAS could also contribute its antimicrobial activity to the overall deactivation efficiency of PQAS–AgNPs to *B. subtilis*. Some researchers have investigated the antimicrobial ability of PQAS. Chen *et al.* found that quaternary ammonium salts could significantly improve the antimicrobial effect, and had strong inactivation effect on *E. coli* and *S. aureus*.[34] Huang *et al.* added chitosan quaternary ammonium salt to the nanofiltration membrane, and found that the filter membrane had better antibacterial properties during filtration process.[35] The antibacterial activity of PQAS on *B. subtilis* was also studied in our test with PVP as reference. As illustrated in

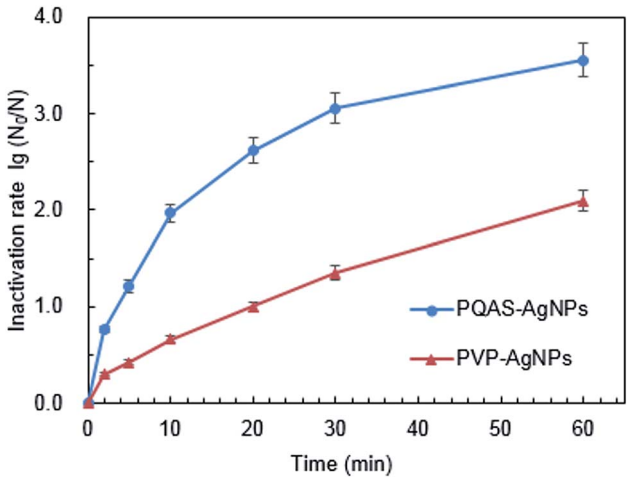

Fig. 2 Inactivation efficiency of *B. subtilis* by PQAS–AgNPs and PVP-AgNPs. Reaction conditions: [AgNPs] = 10.0 mg L^{-1}, pH = 7.1, T = 25 °C, initial concentration of bacteria: 10^6 CFU mL^{-1}.

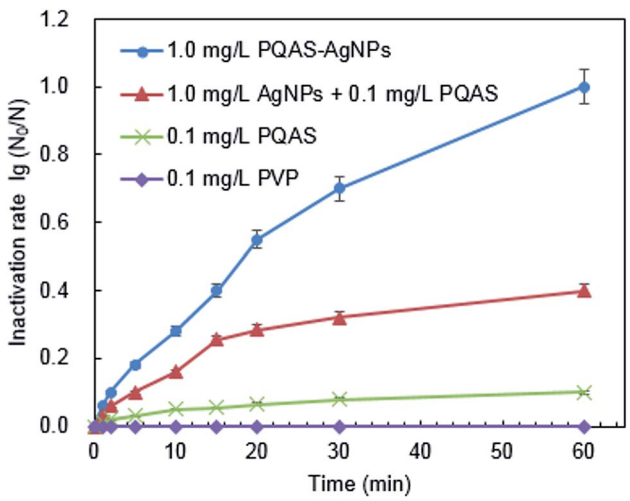

Fig. 3 The role of PQAS and AgNPs in the antibacterial activity of PQAS–AgNPs. Reaction conditions: reaction time = 60 min, pH = 7.1, T = 25 °C, initial concentration of *B. subtilis*: 10^6 CFU mL^{-1}.

Fig. 3, PVP showed no any deactivation activity. While PQAS exhibited antibacterial activity on *B. subtilis*, and 0.1 log of *B. subtilis* was deactivated in the presence of 0.1 mg L^{-1} of PQAS in 60 min. Here a question, whether the antibacterial capacity of PQAS–AgNPs was just the simple summation of the antibacterial activities of PQAS and AgNPs or not, should be clarified. Then, the antibacterial activity of 1.0 mg L^{-1} of PQAS–AgNPs was compared with the combination of 0.1 mg L^{-1} PQAS and 1.0 mg L^{-1} of AgNPs. In this experiment, PVP-AgNPs were used to replace the uncoated AgNPs to avoid the poor dispersion of AgNPs alone. Here 1.0 mg L^{-1} nanosilver dosage was applied in order to distinguish the potency of each antimicrobial material, and 0.1 mg L^{-1} PQAS solution was used to simulate the coating concentration of 1.0 mg L^{-1} of PQAS–AgNPs (By measuring the TOC of PQAS–AgNPs, we found that the carbon content of 1.0 mg L^{-1} of PQAS–AgNPs didn't exceed 0.1 mg L^{-1}. In order to facilitate calculation, 0.1 mg L^{-1} PQAS was used to simulate the surface coating content of 1.0 mg L^{-1} of PQAS–AgNPs.) The comparison results were shown in Fig. 3. It was worthy to note that the deactivation efficiency of 1.0 mg L^{-1} of PQAS–AgNPs on *B. subtilis* was much higher than that of the summation of 0.1 mg L^{-1} PQAS and 1.0 mg L^{-1} of AgNPs, which indicated that the synergistic antibacterial effect should occur between PQAS and AgNPs. It was inferred that positive charge surface of PQAS might facilitate the contact of *B. subtilis* with AgNPs, which improved the antimicrobial performance of PQAS–AgNPs.

In addition, the role of the dissolution of metallic ions on the antibacterial capacity of PQAS–AgNPs must be taken into consideration. Many researchers proposed that the release of silver ions from AgNPs was the key to their antimicrobial ability.[36–38] The different antibacterial capacity between PQAS–AgNPs and PVP-AgNPs might relate to the different dissolution of silver ions. The release of silver ions from 1.0 mg L^{-1} of PQAS–AgNPs and PVP-AgNPs after 60 min was studied. As shown in Fig. 4, there was no significant difference of silver ions dissolution. The silver ions released from PQAS–AgNPs and PVP-AgNPs were 4.3 μg L^{-1} and 4.1 μg L^{-1}, respectively. The antimicrobial rate of 4.3 μg L^{-1} and 4.1 μg L^{-1} of silver ions were no more than 0.1 log (Fig. S2†). The antimicrobial rate of 4.3 μg L^{-1} of silver ions occupied only 10.0% of the antimicrobial rate of 1.0 mg L^{-1} of PQAS–AgNPs. And a conclusion could be obtained that the antibacterial process of PQAS–AgNPs was mainly the surface interaction of *B. subtilis* with PQAS–AgNPs.

3.3 Influencing factors

3.3.1 Effect of the dose of antibacterial material. Effect of antibacterial material dosage on inactivation efficiency was investigated by conducting inactivation experiments at different PQAS–AgNPs concentrations (1.0, 2.0, 5.0 and 10.0 mg L^{-1}). Fig. 5 showed that higher dosage of PQAS–AgNPs led to higher antibacterial efficiency, and the inactivation efficiency of *B. subtilis* with 10.0 mg L^{-1} of PQAS–AgNPs in 15 min was six times of that with 1.0 mg L^{-1} of PQAS–AgNPs. In order to further check the role of AgNPs (taking PVP-AgNPs as a replacement) and PQAS for the antibacterial capacity of PQAS–AgNPs, the antibacterial efficiencies of 1.0, 2.0, 5.0 and 10.0 mg L^{-1} of AgNPs and 0.1, 0.2, 0.5 and 1.0 mg L^{-1} of PQAS, which corresponded to the concentration of PQAS in 1.0, 2.0, 5.0 and 10.0 mg L^{-1} PQAS–AgNPs, were also tested (Fig. 5). The antibacterial efficiencies of PQAS and AgNPs along increased with the increasing of their dosages, while the antibacterial efficiencies of the summation of AgNPs and PQAS were still less than those of PQAS–AgNPs, which further proved the synergistic effect of PQAS and AgNPs. And as illustrated in Table 1, it was interesting to observe that the antibacterial efficiency ratios of AgNPs to PQAS–AgNPs and the summation of AgNPs and PQAS to PQAS–AgNPs both became lower at higher dosage of PQAS–AgNPs, which indicated that higher PQAS–AgNPs dosing could result in more significant synergistic effect. This should be the result of the more adsorption sites for bacteria on the surface of PQAS–AgNPs at higher dosage of PQAS–AgNPs, which then benefited the antibacterial interaction.

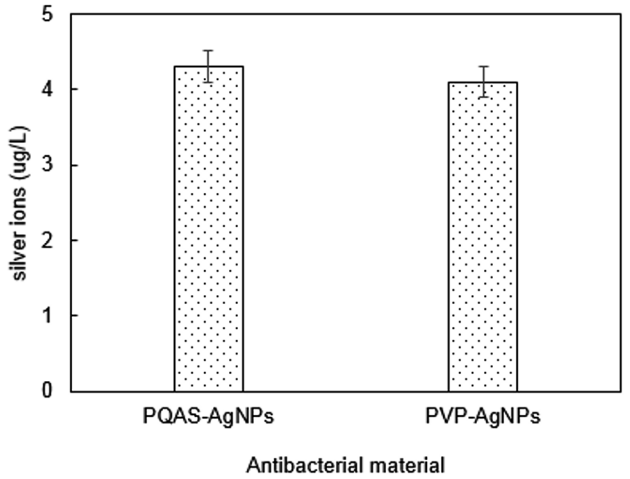

Fig. 4 The silver ion release in PQAS–AgNPs or PVP-AgNPs solution. Reaction conditions: [AgNPs] = 1.0 mg L^{-1}, reaction time = 60 min, pH = 7.1, T = 25 °C.

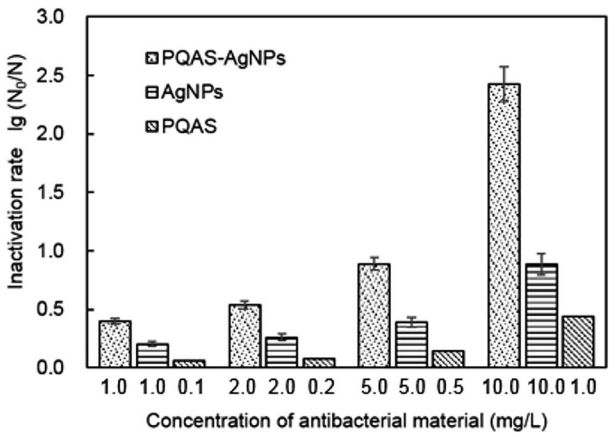

Fig. 5 Inactivation efficiency of *B. subtilis* by different doses of PQAS–AgNPs, AgNPs and PQAS. Reaction conditions: reaction time = 15 min, pH = 7.1, T = 25 °C, initial concentration of bacteria: 10^6 CFU mL^{-1}.

Table 1 The ratio of inactivation rate of AgNPs/PQAS–AgNPs and (AgNPs + PQAS)/PQAS–AgNPs[a]

Dosage of antibacterial materials (mg L^{-1})	A* 1.0	B* 1.0	C* 0.1	A* 2.0	B* 2.0	C* 0.2	A* 5.0	B* 5.0	C* 0.5	A* 10.0	B* 10.0	C* 1.0
Inactivation rate (log)	0.400	0.200	0.055	0.540	0.260	0.078	0.885	0.390	0.138	2.425	0.885	0.437
Ratio of inactivation rate of B*/A*	0.500			0.481			0.441			0.365		
Ratio of inactivation rate of (B* + C*)/A*	0.638			0.626			0.597			0.545		

[a] A* represented PQAS–AgNPs, B* represented AgNPs, C* represented PQAS.

3.3.2 Effect of pH. The surface electrical property of PQAS–AgNPs and the target bacteria as well as the dissolution of silver might be affected under different pH conditions, which should result in different deactivation performance, so the effect of pH on the antimicrobial activity of PQAS–AgNPs was studied in this study. The experiments were carried out under pH values ranging about from 5.0 to 9.0 based on the consideration of the effect of pH on bacterial activity itself. The pre-test showed that the activity of *B. subtilis* was stable in the pH range studied. As illustrated in Fig. 6, the deactivation of *B. subtilis* was affected by pH condition. In the range of pH studied, the bactericidal rate was the highest under acidic condition, followed with neutral condition, and the weakest bactericidal rate was under alkaline condition.

The surface potential of PQAS–AgNPs and *B. subtilis* at different pH was analyzed. The ζ potentials of PQAS–AgNPs at pH 4.9, 7.1 and 8.9 were +31.0, +30.8 and +22.0 mV, respectively. In neutral and weak acidic environment, the ζ potential of PQAS–AgNPs had little difference. However, in weak alkaline environment, the surface potential of PQAS–AgNPs decreased, which should be due to the adsorption of OH^- on the surface of PQAS–AgNPs. At pH 4.9, 7.1 and 8.9, the ζ potentials of *B. subtilis* were measured to be −38.1, −40.5 and −44.3 mV, respectively. The potential differences between antimicrobial material and bacteria were 68.1 mV, 71.3 mV and 66.3 mV under pH 4.9, 7.1 and 8.9, respectively. The potential difference was the largest under neutral condition. Greater potential difference between PQAS–AgNPs and *B. subtilis* at pH 7.1 than that at pH 8.9 should be the reason of higher deactivation efficiency of *B. subtilis* at pH 7.1. The abnormally higher deactivation capacity of PQAS–AgNPs at pH 4.9, which should display the lower deactivation rate than that at pH 7.1 from the consideration of the potential differences of between PQAS–AgNPs and *B. subtilis* at pH 4.9 and 7.1, should be due to the contribution of the dissolved silver ions. The concentration of dissolved silver ions was 173.0 μg L^{-1} at pH 4.9, which was more than five times of that at pH 7.1 and 8.9 (34.2 and 31.8 μg L^{-1} at pH 7.1 and 8.9, respectively, Fig. 7). The deactivation activity of 173.0, 34.2 and 31.8 μg L^{-1} of silver ions was also tested. As shown in Fig. S3,† the deactivation efficiency of *B. subtilis* in the presence of 173.0 μg L^{-1} of silver ions (the corresponding concentration of silver ions dissolved at pH 4.9) was 3.1 times higher than that in the presence of 34.6 μg L^{-1} of silver ions (the corresponding concentration of silver ions dissolved at pH 7.1). And the ratio of the deactivation rate of 173.0 μg L^{-1} of silver ions to 10.0 mg L^{-1} of PQAS–AgNPs was 38.0%, which suggested that at acidic condition, the silver ions in the solution also played an important role for the deactivation of *B. subtilis* besides the surface deactivation of PQAS–AgNPs.

3.3.3 Effect of Cl^-. The presence of chlorine ions was reported to affect the stability of AgNPs and the dissolution of silver ions, which might result in the change of their antimicrobial capacities.[39,40] In this work, the effect of Cl^- on the antimicrobial reactivity of PQAS–AgNPs was investigated. As

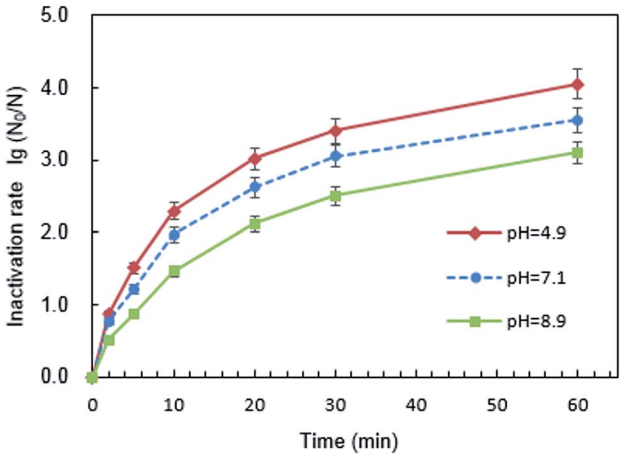

Fig. 6 Inactivation efficiency of *B. subtilis* with PQAS–AgNPs of different pH values (pH = 4.9, 7.1, 8.9). Reaction conditions: [AgNPs] = 10.0 mg L^{-1}, reaction time = 60 min, T = 25 °C, initial concentration of *B. subtilis*: 10^6 CFU mL^{-1}.

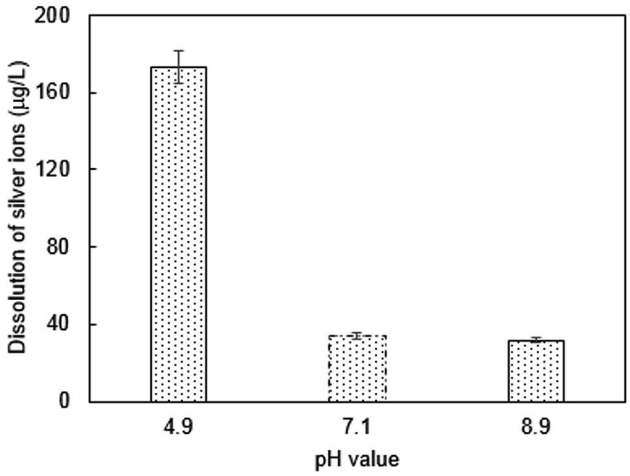

Fig. 7 Dissolution of silver ions in PQAS–AgNPs under different pH values. Reaction conditions: [AgNPs] = 10.0 mg L^{-1}, reaction time = 60 min, T = 25 °C.

shown in Fig. 8(a), the presence of Cl^- weakened the antimicrobial effect of PQAS–AgNPs, and with the increase of chloride concentration, the inhibition effect was more obvious. The effect of Cl^- on the antimicrobial reactivity of PQAS and AgNPs (with PVP-AgNPs as a replacement) was also investigated. The results showed that chloride ion had no effect on the antimicrobial activity of PQAS (Fig. S4†). While, the presence of Cl^- resulted in the decrease of the antimicrobial activity of AgNPs, which was shown in Fig. S5.† Compared with PQAS–AgNPs, the presence of chlorine ions exhibited more significant weakening effect on the deactivation of *B. subtilis*. In the presence of 10.0 mM of Cl^-, the inactivation rate of PQAS–AgNPs to *B. subtilis* decreased from 3.55 log to 3.07 log, and the antimicrobial effect decreased by 13.51%, while the inactivation rate of PVP-AgNPs to *B. subtilis* decreased by 36.57%. This should be due to unaffected antimicrobial reactivity of PQAS and the synergistic antimicrobial effect in PQAS–AgNPs.

Li *et al.* showed that the stability of AgNPs was strongly affected by the presence of Cl^-, and the increase of the concentration of Cl^- led to a corresponding increase in the aggregation rate.[41] Chambers found that chloride might cause the formation of $AgCl^0(s)$ shells and bridging between AgNPs, thus AgNP aggregates were formed.[40] In our study, as illustrated in Fig. 8(b), when Cl^- was added, the ultraviolet absorption spectrum unchanged compared with that in the absence of Cl^-, and the peak height and peak shape were well, which indicated that the particle size of PQAS–AgNPs did not change, and no agglomeration occurred. This result also suggested that stability of PQAS–AgNPs was not just dependent on the electrostatic repulsion effect, but also on the space steric effect.[42]

The effect of Cl^- on the dissolution of nanoparticles was not conclusive. Li *et al.* found that the formation of a AgCl layer on the AgNPs inhibited their dissolution at the presence of 10–40 mM NaCl.[41] However, chambers found that AgNP dissolution strongly increased under increased chloride conditions, but the dominant, theoretical, equilibrium aqueous silver species shifted to negatively charged $AgCl_x^{(x-1)-}$ species, which appeared to be less toxic to *E. coli*.[40] The effect of the presence of Cl^- on the dissolution of silver ions from PQAS–AgNPs was studied. It was shown that the dissolution of silver was inhibited in the presence of chloride ions. In 60 min, 34.2 μg L^{-1} of silver ions was detected originally (Fig. 7), while only 18.5 μg L^{-1} of silver ions was dissolved from 10.0 mg L^{-1} of PQAS–AgNPs in the presence of 10.0 mM Cl^- under the same experimental conditions. This might be due to the formation of AgCl on the surface of PQAS–AgNPs which hindered the dissolution of silver ions. And the formation of AgCl should also occur on the surface of PQAS–AgNPs and then lead to the decrease of the effective antibacterial sites, which might be a key reason to the weakening of the antibacterial reactivity of PQAS–AgNPs in the presence of Cl^-.

3.3.4 Effect of HA. To understand the effect of organic matters, the influence of HA on the inactivation efficiency of PQAS–AgNPs to *B. subtilis* was shown in Fig. 9. After HA was added, the inactivation effect of PQAS–AgNPs on bacteria decreased significantly, and the degree of reduction was more obvious with the increase of HA concentration. Specifically, the inactivation rate decreased from 3.55 log to 1.15 log after adding 20.0 mg L^{-1} HA to PQAS–AgNPs antibacterial system for 1 h reaction. As a comparison, the results of inactivation effect of PVP-AgNPs was illustrated in Fig. S6.† After 20.0 mg L^{-1} of HA was added for 60 min reaction, the antimicrobial activity of PVP-AgNPs decreased by 0.82 log (39.2%), while that of PQAS–AgNPs decreased by 2.40 log (67.6%). It was noteworthy that HA had a more conspicuous weakening effect to the inactivation reactivity of PQAS–AgNPs than PVP-AgNPs.

The presence of HA was supposed to affect the property of both AgNPs and PQAS. Combining with the previous literatures, it could be known that HA weakened the antimicrobial ability of PQAS–AgNPs as the following reasons: (1) the basic structure of HA was aromatic and aliphatic rings, connecting with carboxyl, hydroxyl and carbonyl groups. It could adsorb on the surface of

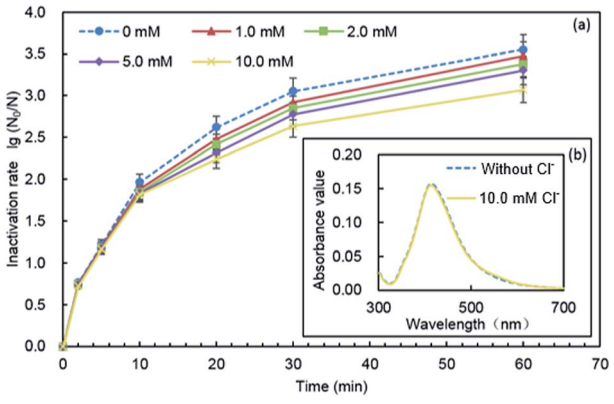

Fig. 8 (a) Effect of Cl^- on antibacterial efficacy to *B. subtilis* of PQAS–AgNPs. (b) Ultraviolet absorption spectra of PQAS–AgNPs in electrolyte solution. Reaction conditions: [AgNPs] = 10.0 mg L^{-1}, contact time = 60 min, pH = 7.1, T = 25 °C, initial concentration of *B. subtilis*: 10^6 CFU mL^{-1}.

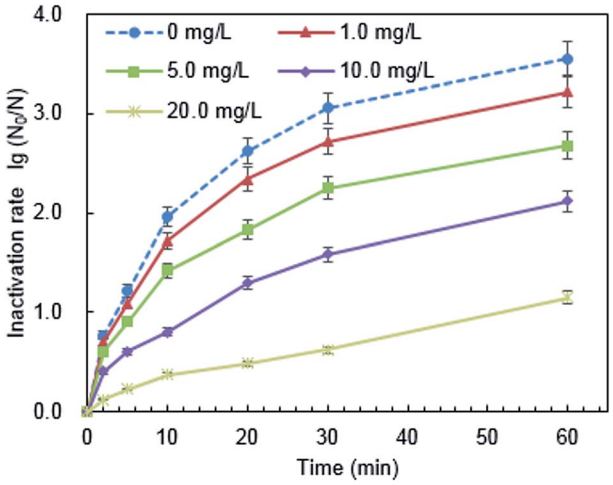

Fig. 9 Effect of HA on antibacterial efficacy to *B. subtilis* with PQAS–AgNPs. Reaction conditions: [AgNPs] = 10.0 mg L^{-1}, reaction time = 60 min, pH = 7.1, T = 25 °C, initial concentration of *B. subtilis*: 10^6 CFU mL^{-1}.

antimicrobial materials and bacteria and hinder the contact between cells and nanoparticles;[39,43] (2) the presence of HA reduced the positive charge on the surface of the antimicrobial material, thus weakening the electrostatic attraction between the material and bacteria. We measured the ζ potential of PQAS–AgNPs and VP-AgNPs in the presence of HA, and found that the surface potential of PQAS–AgNPs and PVP-AgNPs decreased from +30.8 mV to −29.7 mV and from −9.3 mV to −27.2 mV, respectively. It was interesting to found that the decrease degree of surface potential of PQAS–AgNPs was more significantly than that of PVP-AgNPs, which might be one of the reasons that the antibacterial capacity of PQAS–AgNPs were weakened more seriously by HA; (3) the presence of HA might hinder the antibacterial effect of silver ions released from nano-silver. The reducibility of HA could reduce silver ions to silver monomers.[44] In addition, silver ions might form complexes with HA,[45,46] resulting in a reduction of antibacterial effectiveness; (4) Jeen-Kuan Chen reported that chitosan had potent adsorption capacity to HA.[47] In this experiment, PQAS was obtained by modifying a quaternary ammonium salt with the chitosan polymer as a skeleton. Therefore, we speculated that PQAS and HA could also crosslink together due to the interaction of various groups, thus affecting the antibacterial properties of PQAS itself. More work was needed in the future to confirm this hypothesis.

3.4 Damage to *B. subtilis* cells

3.4.1 Injury to cell membrane (FCM results). In FCM detection, the change of cell permeability was reflected by the fluorescence position shift of the bacteria cluster, and FCM could quantitatively analyze the ratio of survival and death of bacteria.[26] As could be seen from Fig. 10, with the increase of PQAS–AgNPs concentration, the live bacteria ratio diminished gradually, resulting in the shifts of the clusters towards the left away from the fixed live-gate. This indicated that the inactivation of silver nanoparticles enhanced and the selective permeability of cell membranes lost continuously.[48]

Comparing the same concentration of PQAS–AgNPs and PVP-AgNPs (Fig. S7†), it was found that with the increase of the concentration of antimicrobial materials, the difference of the ratio of dead/live bacteria increased gradually (Fig. S8†). When the material concentration reached 10.0 mg L^{-1}, the ratio of dead/live bacteria was 42.9 in the FCM results of bacteria treated with PQAS–AgNPs, while the ratio of PVP-AgNPs was 13.8. This ratio also showed that the destruction of bacterial cell membrane by PQAS–AgNPs was greater than that by PVP-AgNPs.

3.4.2 Determination the ATP changes of cells. ATP was a key energy carrier, which could serve as an indicator of viability, and ATP level could also reflect a microbial concentration.[27] At the same time, as an intracellular substance, the presence of ATP outside the cell could reflect the loss of intracellular substances and the functional integrity of the cell wall and cell membrane. The ATP changes of bacteria treated with PQAS–AgNPs were shown in Fig. 11. When PQAS–AgNPs inactivated bacteria, the cell wall and cell membrane of bacteria were destroyed. With the increase of PQAS–AgNPs dosage, the

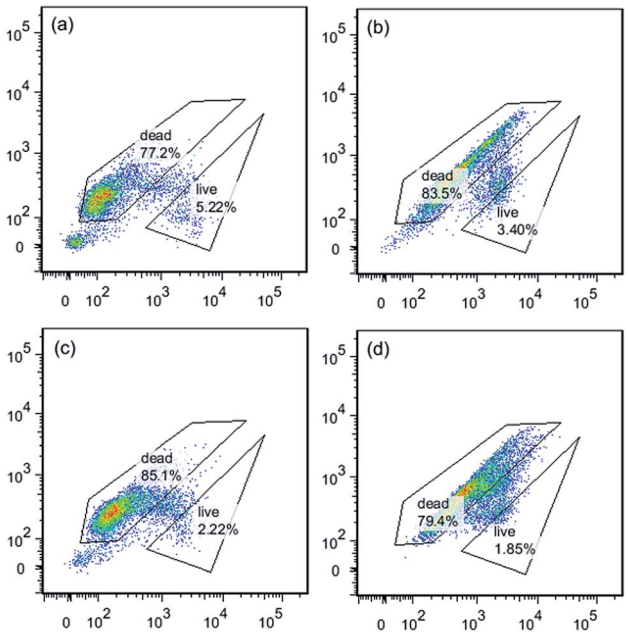

Fig. 10 FCM results of *B. subtilis* after treated by PQAS–AgNPs. Among them, (a)–(d) represent the concentration of PQAS–AgNPs is 1.0, 2.0, 5.0, 10.0 mg L^{-1}, respectively. Reaction conditions: reaction time = 15 min, pH = 7.1, T = 25 °C, initial concentration of *B. subtilis*: 10^6 CFU mL^{-1}.

ATP content of *B. subtilis* showed a consistent trend. The total amount of ATP in cells showed a downward trend, mainly because nano-silver destroyed the respiratory chain of cells, reduced the synthesis of ATP,[49,50] and also indicated the decrease of bacterial activity. The proportion of extracellular ATP showed an increasing trend and the proportion of intracellular ATP showed a downward trend, indicating that the intracellular substances was leaked out and the cell wall and cell membrane function were destroyed.

By comparing the differences between PQAS–AgNPs and PVP-AgNPs (Fig. S9†), it could be found that the ratio of

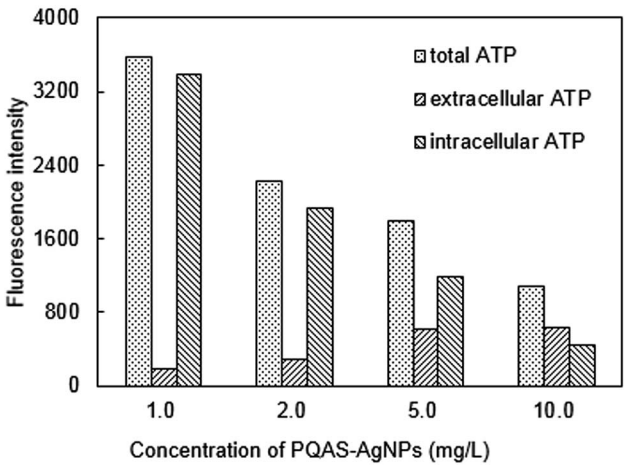

Fig. 11 Changes of ATP of *B. subtilis* after treated by PQAS–AgNPs. Reaction conditions: reaction time = 15 min, pH = 7.1, T = 25 °C, initial concentration of *B. subtilis*: 10^6 CFU mL^{-1}.

extracellular ATP/intracellular ATP after PQAS–AgNPs treatment was significantly higher than that treated with PVP-AgNPs at the same concentration. When bacteria were treated with 10.0 mg L^{-1} PQAS–AgNPs, the extracellular ATP content was 144.2% of intracellular ATP content, whereas that of PVP-AgNPs was only 34.8% (as Fig. S10† showed), indicating that PQAS–AgNPs treatment made the leakage of intracellular substances more serious and caused more severe damage to the cell wall and cell membrane structure.

4 Conclusions

In this study, polymer quaternary ammonium salt–capped silver nanoparticles (PQAS–AgNPs) were synthesized and tested for their antimicrobial activities. The results showed that PQAS–AgNPs revealed excellent antimicrobial activity to *B. subtilis*. The positive surface, the antimicrobial activity of PQAS, and the synergistic antibacterial effect between PQAS and AgNPs contributed to the significant antibacterial superiority of PQAS–AgNPs. The antimicrobial efficiency of PQAS–AgNPs to *B. subtilis* was affected by the dose of the material, pH, Cl^- and HA in water. The antimicrobial efficacy of PQAS–AgNPs was stronger at lower pH condition. The impact of the dose of the material was positive, whereas the effects of Cl^- and HA were negative. In combination with the results of FCM and ATP content, it was found that PQAS–AgNPs destroyed the respiratory chain of cells, reduced the synthesis of ATP, and destroyed the cell wall and cell membrane function which led to the leaking of the intracellular substances.

Conflicts of interest

There are no conflicts to declare.

Acknowledgements

This study was supported by the National Natural Science Foundation of China (Grant 51478322, 51278351), and the Major National Water Pollution Control and Management Project (Grant 2014ZX07405-003, 2017ZX07201001).

Notes and references

1 J. Lu, T. Zhang, J. Ma and Z. Chen, *J. Hazard. Mater.*, 2009, **162**, 140–145.
2 Y. Kargalioglu, B. J. McMillan, R. A. Minear and M. J. Plewa, *Teratog., Carcinog., Mutagen.*, 2002, **22**, 113–128.
3 E. D. Wagner and M. J. Plewa, *J. Environ. Sci.*, 2017, **58**, 64–76.
4 S. Sciacca and G. O. Conti, *Mediterr. J. Nutr. Metab.*, 2009, **2**, 157–162.
5 M. Greenberg, *Am. J. Ind. Med.*, 1992, **21**, 137–139.
6 S. Pigeot-Rémy, F. Simonet, E. Errazuriz-Cerda, J. C. Lazzaroni, D. Atlan and C. Guillard, *Appl. Catal., B*, 2011, **104**, 390–398.
7 Q. Zhang, R. Ma, Y. Tian, B. Su, K. Wang, S. Yu, J. Zhang and J. Fang, *Environ. Sci. Technol.*, 2016, **50**, 3184–3192.
8 F. Hossain, O. J. Perales-Perez, S. Hwang and F. Román, *Sci. Total Environ.*, 2014, **466–467**, 1047–1059.
9 P. Gong, H. Li, X. He, K. Wang, J. Hu, W. Tan, S. Zhang and X. Yang, *Nanotechnology*, 2007, **18**, 285604.
10 T. A. Dankovich and D. G. Gray, *Environ. Sci. Technol.*, 2011, **45**, 1992–1998.
11 M. Guzman, J. Dille and S. Godet, *Nanomedicine*, 2012, **8**, 37–45.
12 T. D. Huang, M. H. Sui and J. Y. Li, *Sci. Total Environ.*, 2017, **574**, 818–828.
13 J. Z. Ma, J. T. Zhang, Z. G. Xiong, Y. Yong and X. S. Zhao, *J. Mater. Chem.*, 2011, **21**, 3350–3352.
14 X. R. Xie, W. Cong, F. Zhao, H. J. Li, W. Y. Xin, G. G. Hou and C. H. Wang, *J. Enzyme Inhib. Med. Chem.*, 2017, **33**, 98–105.
15 C. Zhang, F. Cui, G.-m. Zeng, M. Jiang, Z.-z. Yang, Z.-g. Yu, M.-y. Zhu and L.-q. Shen, *Sci. Total Environ.*, 2015, **518–519**, 352–362.
16 S. M. Iconomopoulou and G. A. Voyiatzis, *J. Controlled Release*, 2005, **103**, 451–464.
17 B. Dizman, M. O. Elasri and L. J. Mathias, *J. Appl. Polym. Sci.*, 2004, **94**, 635–642.
18 G. Lu, D. Wu and R. Fu, *React. Funct. Polym.*, 2007, **67**, 355–366.
19 Y. Xue, H. Xiao and Y. Zhang, *Int. J. Mol. Sci.*, 2015, **16**, 3626.
20 R. Sinha, R. Karan, A. Sinha and S. K. Khare, *Bioresour. Technol.*, 2011, **102**, 1516–1520.
21 A. Huertas, B. Barbeau, C. Desjardins, A. Galarza, M. A. Figueroa and G. A. Toranzos, *Water Sci. Technol.*, 2003, **47**, 255–259.
22 B. Setlow, K. A. McGinnis, K. Ragkousi and P. Setlow, *J. Bacteriol.*, 2000, **182**, 6906–6912.
23 M. Cho, J.-H. Kim and J. Yoon, *Water Res.*, 2006, **40**, 2911–2920.
24 M. A. Larson and B. J. Mariñas, *Water Res.*, 2003, **37**, 833–844.
25 Y. O. Thomas, W. J. Lulves and A. A. Kraft, *J. Food Sci.*, 1981, **46**, 1951–1952.
26 J. Y. Wang, M. H. Sui, B. J. Yuan, H. W. Li and H. T. Lu, *Sci. Total Environ.*, 2019, **648**, 271–284.
27 F. Hammes, F. Goldschmidt, M. Vital, Y. Y. Wang and T. Egli, *Water Res.*, 2010, **44**, 3915–3923.
28 L. Li, J. Sun, X. R. Li, Y. Zhang, Z. X. Wang, C. R. Wang, J. W. Dai and Q. B. Wang, *Biomaterials*, 2012, **33**, 1714–1721.
29 D. Teng-Yuan, C. Wei-Ting, W. Ching-Wen, C. Chiao-Pei, C. Chen-Ni, L. Ming-Cheng, S. Jenn-Ming, C. In-Gann and K. Tzu-Hsuan, *Phys. Chem. Chem. Phys.*, 2009, **11**, 6269–6275.
30 Y.-M. Long, L.-G. Hu, X.-T. Yan, X.-C. Zhao, Q.-F. Zhou, Y. Cai and G.-B. Jiang, *Int. J. Nanomed.*, 2017, **12**, 3193–3206.
31 H. Wang, X. Qiao, J. Chen, X. Wang and S. Ding, *Mater. Chem. Phys.*, 2005, **94**, 449–453.
32 V. P. Harden and J. O. Harris, *J. Bacteriol.*, 1953, **65**, 198.
33 A. M. El Badawy, R. G. Silva, B. Morris, K. G. Scheckel, M. T. Suidan and T. M. Tolaymat, *Environ. Sci. Technol.*, 2011, **45**, 283–287.
34 Y. X. Chen, J. N. Li, Q. Q. Li, Y. Y. Shen, Z. C. Ge, W. W. Zhang and S. G. Chen, *Carbohydr. Polym.*, 2016, **143**, 246–253.
35 R. H. Huang, G. H. Chen, M. K. Sun, Y. M. Hu and C. J. Gao, *J. Membr. Sci.*, 2006, **286**, 237–244.

36 W.-R. Li, X.-B. Xie, Q.-S. Shi, H.-Y. Zeng, Y.-S. OU-Yang and Y.-B. Chen, *Appl. Microbiol. Biotechnol.*, 2010, **85**, 1115–1122.
37 Z.-m. Xiu, Q.-b. Zhang, H. L. Puppala, V. L. Colvin and P. J. J. Alvarez, *Nano Lett.*, 2012, **12**, 4271–4275.
38 S. J. Lia, Y. P. Zhang, X. H. Pan, F. Z. Zhu, C. Y. Jiang, Q. Q. Liu, Z. Y. Cheng, G. Dai, G. J. Wu, L. Q. Wang and L. Y. Chen, *Int. J. Nanomed.*, 2019, **14**, 1469–1487.
39 T. D. Huang, M. H. Sui, X. Yan, X. Zhang and Z. Yuan, *Colloids Surf., A*, 2016, **509**, 492–503.
40 B. A. Chambers, A. R. M. N. Afrooz, S. Bae, N. Aich, L. Katz, N. B. Saleh and M. J. Kirisits, *Environ. Sci. Technol.*, 2014, **48**, 761–769.
41 X. Li, J. J. Lenhart and H. W. Walker, *Langmuir*, 2010, **26**, 16690–16698.
42 H. Y. Zhang, J. A. Smith and V. Oyanedel-Craver, *Water Res.*, 2012, **46**, 691–699.
43 K. A. Huynh and K. L. Chen, *Environ. Sci. Technol.*, 2011, **45**, 5564–5571.
44 A. Nelson, R. I. Maccuspie, D. A. Navarro, D. S. Aga, B. Sarbajit, S. Mary and V. K. Sharma, *Environ. Sci. Technol.*, 2011, **45**, 3895–3901.
45 X. Wang, W. Fan, Z. Dong, D. Liang and T. Zhou, *Water Res.*, 2018, **138**, 224–233.
46 S. M. Wirth, G. V. Lowry and R. D. Tilton, *Environ. Sci. Technol.*, 2012, **46**, 12687–12696.
47 J. K. Chen, C. H. Yeh, L. C. Wang, T. H. Liou, C. R. Shen and C. L. Liu, *Mar. Drugs*, 2011, **9**, 2488–2498.
48 Y. Lee, S. Imminger, N. Czekalski, U. von Gunten and F. Hammes, *Water Res.*, 2016, **101**, 617–627.
49 C. N. Lok, C. M. Ho, R. Chen, Q. Y. He, W. Y. Yu, H. Z. Sun, P. K. H. Tam, J. F. Chiu and C. M. Che, *J. Proteome Res.*, 2006, **5**, 916–924.
50 P. V. AshaRani, G. Low Kah Mun, M. P. Hande and S. Valiyaveettil, *ACS Nano*, 2009, **3**, 279–290.